

The anomalously low (sub)millimeter spectral indices of some protoplanetary disks may be explained by dust self-scattering

HAUYU BAOBAB LIU<sup>1</sup>

<sup>1</sup>Academia Sinica Institute of Astronomy and Astrophysics, P.O. Box 23-141, Taipei 10617, Taiwan

## ABSTRACT

Previous (sub)millimeter observations have found that the spectral indices of dust emission from some young stellar objects are lower than that of the black body emission in the Rayleigh-Jeans limit (i.e., 2.0). In particular, the recent Atacama Large Millimeter Array observations have spatially resolved that the innermost regions of the protoplanetary disks TW Hya and HD 163296 present anomalously low (i.e., <2.0) millimeter spectral indices. In some previous works, such anomalously low millimeter spectral indices were considered unphysical and were attributed to measurement errors. The present work clarifies that if the albedo is high and is increasing with frequency, it is possible to reproduce such anomalously low spectral indices when the emission source is optically thick. In addition, to yield lower than 2.0 spectral index at (sub)millimeter bands, the required dust maximum grain size  $a_{\max}$  is on the order of 10-100  $\mu\text{m}$ , which is very well consistent with the previously derived  $a_{\max}$  values based on multi-wavelength dust polarimetric observations. In light of this, measuring Stokes I spectral index may also serve as an auxiliary approach for assessing whether the observed dust polarization is mainly due to dust scattering or is due to the aligned dust grains.

*Keywords:* stars: individual (TW Hya) — protoplanetary disks

## 1. INTRODUCTION

It has been widely applied to approximate interstellar dust emission with the so called modified black body formulation (for a review see Hildebrand 1983)

$$S_{\nu} = \Omega B_{\nu}(T_{\text{dust}})(1 - e^{-\tau_{\nu}}),$$

where  $S_{\nu}$  is the observed flux at frequency  $\nu$ ,  $\Omega$  is the solid angle of the emission region,  $B_{\nu}(T_{\text{dust}})$  is the Planck function at dust temperature  $T_{\text{dust}}$  and frequency  $\nu$ , and  $\tau_{\nu}$  is the optical depth of dust. Dust optical depth  $\tau_{\nu}$  is further expressed by the product of the dust mass absorption opacity ( $\kappa_{\nu}^{\text{abs}}$ ) and dust mass surface density ( $\Sigma$ ). Owing to that dust grains cannot emit or absorb efficiently at wavelengths which are much longer than their size, at (sub)millimeter bands,  $\kappa_{\nu}^{\text{abs}}$  is proportional to  $(\nu)^{\beta}$ , where  $\beta$  is known as the dust opacity spectral index. The value of  $\beta$  is  $\sim 2$  in the diffuse interstellar medium (ISM) around the solar neighborhood. With the presence of grown dust, the value of  $\beta$  can become as low as 0.0. In the Rayleigh-Jeans limit, the observed (sub)millimeter spectral index ( $\alpha$ ) is related to  $\beta$  by  $\alpha = \beta + 2$ .

Corresponding author: Hauyu Baobab Liu  
 hyliu@asiaa.sinica.edu.tw

Some previous (sub)millimeter observations on protoplanetary disks have reported  $\alpha \sim 2.5$ . By assuming that the dust scattering opacity ( $\kappa_{\nu}^{\text{sca}}$ ) is negligible, they argued that  $\beta \sim 0.5$  and suggested that millimeter-sized dust grains may already present in those disks (e.g., Beckwith & Sargent 1991; Carrasco-González et al. 2016, and references therein). However, lately some observations reported anomalously low (sub)millimeter spectral indices ( $\alpha < 2.0$ ), which cannot be reproduced based on the aforementioned formulation (e.g., Class 0/I objects: Jørgensen et al. 2007; Miotello et al. 2014; Li et al. 2017; Liu et al. 2018b; Agurto-Gangas et al. 2019; protoplanetary disks: Tsukagoshi et al. 2016; Liu et al. 2017; Huang et al. 2018; Dent et al. 2019). Due to the significant numbers of such reports, some of which were carried out by teams which possess authority on the technical ground (e.g., Dent et al. 2019), it is hard to attribute all of them to data calibration errors or imaging artifacts. Another related paradox is that the recent, multi-wavelengths polarimetric observations of dust scattering (for more details of this mechanism see Kataoka et al. 2015; Yang et al. 2017) mostly concluded the maximum grain size  $a_{\max} \sim 50\text{-}150 \mu\text{m}$ , which is not yet fully reconciled with those earlier suggestions of millimeter-sized grains based on analyzing spectral indices  $\alpha$  (see Kataoka et al. 2016a,b; Stephens et al. 2017; Bacciotti et al. 2018; Hull et al. 2018).

Based on radiative transfer models, Li et al. (2017) and Galván-Madrid et al. (2018) have argued that when dust

grains are small ( $\ll 1$  mm), the anomalously low  $\alpha$  values can be explained by foreground obscured hot dust. Otherwise, it may be explained by mixing some free-free emission (e.g. Liu et al. 2017). Li et al. (2017) and Galván-Madrid et al. (2018) found that applying foreground obscured hot dust better explains the (sub)millimeter spectral energy distributions (SEDs) of some Class 0/I young stellar objects (YSOs) observed on 100-1000 AU scales.

However, our present understanding is that dust in Class II protoplanetary disks are predominantly heated by protostellar irradiation. Therefore, dust around disk surface is likely hotter than that at disk midplane. If this is indeed the case, then the explanation of foreground obscured hot dust cannot be applied to the Class II protoplanetary disks which are observed in face-on projection. On the other hand, time monitoring observations (e.g., Liu et al. 2014) have shown that the free-free and/or synchrotron emission from Class II protoplanetary disks are rarely bright enough to be able to confuse the measurements of dust emission at (sub)millimeter bands. In light of these, it is particularly puzzling that the less than 2.0 values of  $\alpha$  have been spatially resolved from the inner  $\lesssim 10$  AU radii of the approximately face-on, low-luminosity protoplanetary disk TW Hya (initially reported by Tsukagoshi et al. 2016, and was reproduced by Huang et al. 2018 with independent measurements), and from HD 163296 (Dent et al. 2019).

Based on simplified radiative transfer models, the present work argues that if we take scattering opacity into consideration, it is possible to reproduce the anomalously low  $\alpha$  values at (sub)millimeter bands from an isothermal, high optical depth dust emission source with  $a_{\max} \sim 0.1$  mm. The analysis will be compared with the Atacama Large Millimeter Array (ALMA) observations of the specific Class II protoplanetary disk, TW Hya ( $d \sim 60$  pc; Gaia Collaboration et al. 2016, 2018). Thanks to its approximately face-on projection (for more information of this target source see Qi et al. 2004; Andrews et al. 2016, and references therein), it may be sufficient to consider the analytic solution of radiative transfer equation for a thin slab, without requiring full three-dimensional Monte Carlo radiative transfer modeling. Therefore, the analysis can base on less free parameters and thus the results would be rather comprehensive. In addition, there is less concern with the confusion of free-free emission thanks to the low bolometric luminosity and low protostellar mass of TW Hya.

The observational data utilized in this work are briefly introduced in Section 2.1 while more details are given in Appendix A. The analysis of the SEDs is provided in Section 2.2. Section 3 discusses the general implication of this work to other observational case studies, while our conclusion is nearly identical to the Abstract.

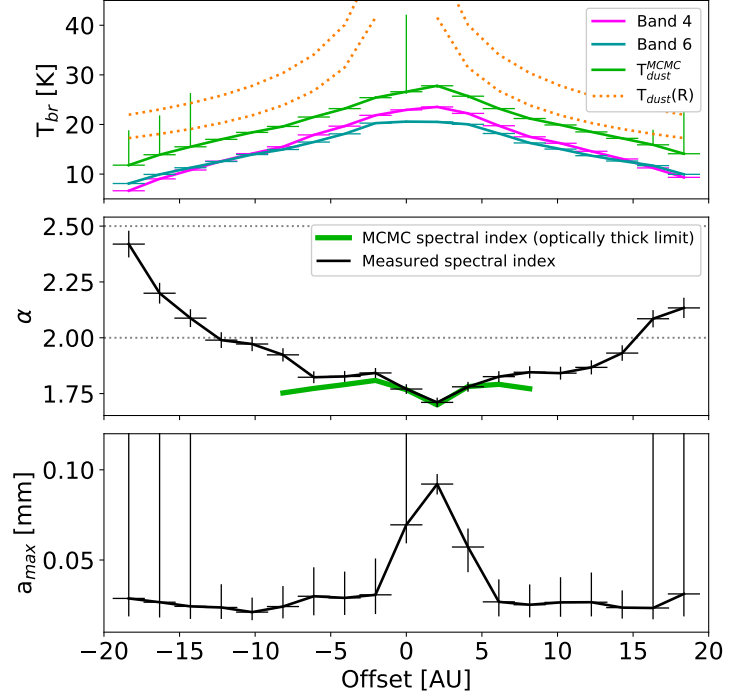


**Figure 1.** Profiles of the dust brightness temperature ( $T_{\text{br}}$ ) observed at Bands 4 and 6 (top), the Band 4-6 spectral indice derived from observations and MCMC fittings ( $\alpha$ ; middle), and the dust temperature  $T_{\text{dust}}^{\text{MCMC}}$  (top) and maximum grain size ( $a_{\max}$ ; bottom) profiles derived from MCMC fittings, which were measured along the major axis of TW Hya (P.A.=155°; positive offset is defined towards the southeast). The vertical error bars of the MCMC fitting results present the 25th and the 75th percentiles. Top panel also shows the power-law  $T_{\text{dust}}(R)=22 \text{ [K]} \times (R/10 \text{ [AU]})^{-0.4}$  and  $28 \text{ [K]} \times (R/10 \text{ [AU]})^{-0.4}$  temperature models suggested by Andrews et al. (2012, 2016).

## 2. DATA ANALYSIS

### 2.1. Millimeter spectral index from TW Hya

The ALMA Band 4 ( $\sim 145$  GHz) and Band 6 ( $\sim 233$  GHz) data taken from project 2015.A.00005.S (PI: Takashi Tsukagoshi), and the ALMA Band 6 data taken from project 2013.1.00114.S (PI: Karin Öberg)<sup>1</sup> were utilized for the present work. These two bands are ideal for the present science purpose due to the sufficiently high dust optical depths, and due to that they can be approximated by the Rayleigh-Jeans limit. The SED analysis can become degenerated when mixing non-Rayleigh-Jeans components is a concern. More details about how the data calibration was reproduced are given in Appendix A.

<sup>1</sup> Note that Tsukagoshi et al. (2016) referred to project 2012.1.00422.S instead of 2013.1.00114.S, which was likely a typo since 2012.1.00422.S did not carry out Band 6 observations.

Top and middle panels of Figure 1 present the dust brightness temperature  $T_{\text{br}}$  and spectral index ( $\alpha$ ) taken from a thin slice along the major axis (P.A.=155°, see Qi et al. 2004; Andrews et al. 2012) of TW Hya. The peak  $T_{\text{br}}$  value detected in this work is lower than that in Tsukagoshi et al. (2016), which is likely due to the poorer angular resolution adopted in this work. In addition, this work did not perform azimuthal averaging to avoid smearing the weakly resolved azimuthal asymmetry at the innermost ring (see Figure 1 of Tsukagoshi et al. 2016; an also see Roberge et al. 2005 for a related claim on large spatial scales). Other than these, the results presented in Figure 1 largely agree with what was presented in Tsukagoshi et al. (2016). The anomalously low (i.e.,  $<2.0$ )  $\alpha$  values were reproduced in the inner  $\sim 10$  AU radii.

## 2.2. Estimating maximum grain sizes based on fitting spectral index

This work adopted the default DSHARP dust optical constants published in Birnstiel et al. (2018), which appears qualitatively similar to what was presented in the independent work Kataoka et al. (2015). The ice-free dust opacity was not considered in this work due to that the detected dust brightness temperature is well below the typically assumed sublimation temperature for water ice (100-200 K). The size averaged dust absorption ( $\kappa_{\nu}^{\text{abs}}$ ) and effective scattering ( $\kappa_{\nu}^{\text{sca,eff}}$ ) opacities were evaluated based on an assumption of spherical compact grains, a power-law grain size distribution with a power-law index  $q=3.5$ , the minimum grain size  $a_{\text{min}}=10^{-4}$  mm and the maximum grain size  $a_{\text{max}}$ , the Mie theory and the Henyey-Greenstein scattering approximation. Figure 2 shows the examples  $\kappa_{\nu}^{\text{abs}}$  and  $\kappa_{\nu}^{\text{sca,eff}}$  for  $a_{\text{max}}=0.01$ , 0.1, 0.15, 1.0, and 10 mm, respectively. From this figure, we can see that dust scattering is negligible when  $a_{\text{max}}$  is  $<0.01$  mm. In addition, at long wavelength  $\kappa_{\nu}^{\text{sca,eff}}$  has steeper slope than  $\kappa_{\nu}^{\text{abs}}$ . When  $a_{\text{max}}$  is close to  $\sim 0.1$  mm,  $\kappa_{\nu}^{\text{sca,eff}}$  becomes comparable with  $\kappa_{\nu}^{\text{abs}}$ , and the curve of  $\kappa_{\nu}^{\text{sca,eff}}$  has an intersection with the curve of  $\kappa_{\nu}^{\text{abs}}$  at the steep slope tail of  $\kappa_{\nu}^{\text{sca,eff}}$  (e.g., at  $\gtrsim 1$  mm wavelengths). Therefore, around this intersection, there is a range of wavelength where the albedo is not negligible and is rapidly decreasing with wavelength. This feature moves to centimeter wavelengths when  $a_{\text{max}} \gtrsim 1$  mm. As a consequence that a higher fraction of dust emission is scattered off at shorter wavelength, at wavelengths close to the aforementioned  $\kappa_{\nu}^{\text{abs}}-\kappa_{\nu}^{\text{sca,eff}}$  intersection, the  $T_{\text{br}}$  of an optically thick isothermal dust slab will increase with wavelength (c.f. Figure 9 of Birnstiel et al. 2018). Figure 3 shows examples of the (sub)millimeter SEDs for various values of  $a_{\text{max}}$ , evaluated based on the analytic radiative transfer solution for such optically thick, isothermal (25 K), geometrically thin dust slab in face-on projection, which was introduced in Birnstiel et al. (2018). They are compared with the ordinary black body SED which has  $\alpha=2.0$  in the Rayleigh-

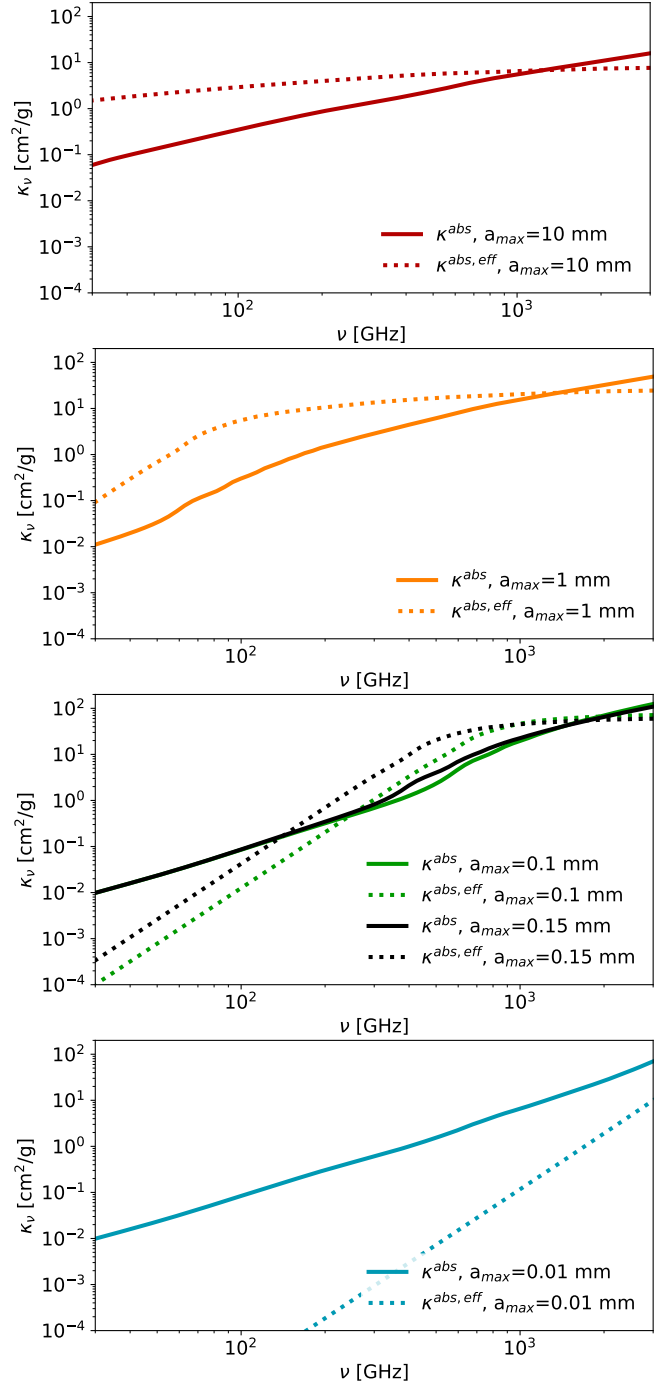


**Figure 2.** Absorption ( $\kappa_{\nu}^{\text{abs}}$ ) and approximated scattering ( $\kappa_{\nu}^{\text{sca,eff}}$ ) opacity of dust derived assuming the DSHARP optical constants (Birnstiel et al. 2018) and a power-law size ( $a$ ) distribution (i.e.,  $n(a) \propto a^{-q}$ ) in between the assumed minimum and maximum grain sizes  $a_{\text{min}}$ ,  $a_{\text{max}}$ . This work adopted the minimum grain size  $a_{\text{min}}=10^{-4}$  mm and the power-law index  $q=3.5$ . From top to bottom panels shows the cases with  $a_{\text{max}}=10$ , 1, 0.1, and 0.01 mm, respectively. The third panel also shows the case with  $a_{\text{max}}=0.15$  mm to demonstrate how the variation rate of albedo may be sensitive to small changes of  $a_{\text{max}}$ .

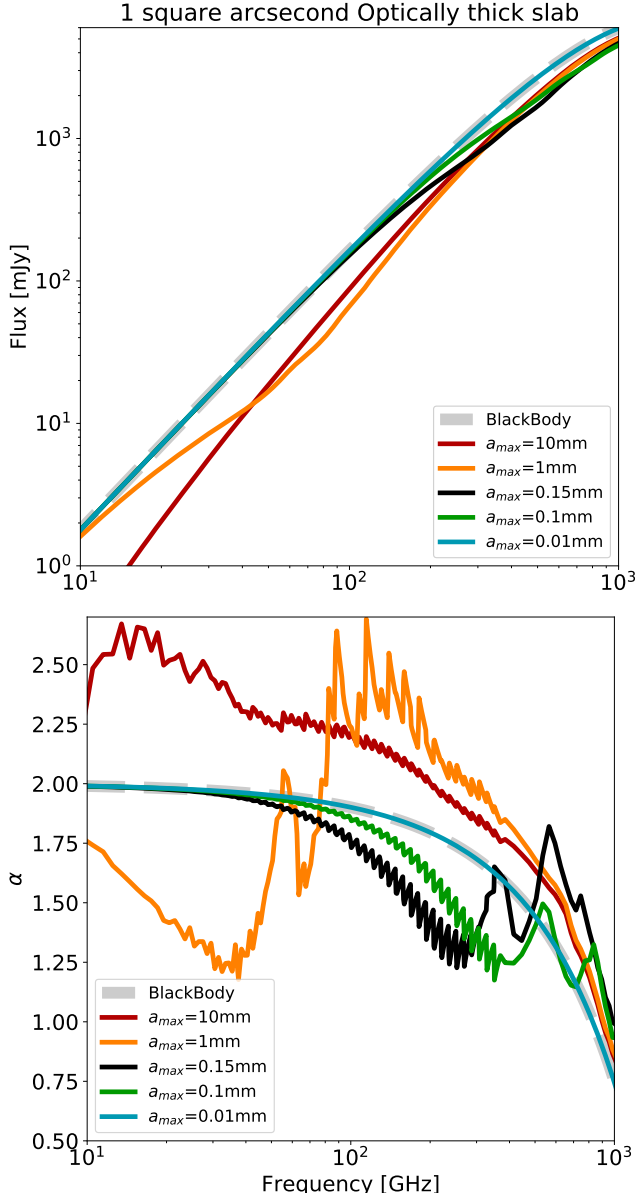


**Figure 3.** Examples of the (sub)millimeter spectral energy distribution (top) and spectral index (bottom) evaluated for optically thick ( $\tau \gg 1$ ) isothermal (25 K) dust slab of 1 square arcsecond angular scales. Gray dashed line shows the case of black body emission. Solid lines show the cases evaluated based on the assumption of DSHARP opacities presented in Figure 2.

Jeans limit. Here we can clearly see that when dust scattering is taken into account, and when  $a_{\max} \sim 0.1$  mm, the anomalously low values  $\alpha < 2.0$  is reproduced at millimeter wavelengths, manifesting with a flatter SED than that of the ordinary black body. The feature of anomalously low  $\alpha$  shifts to centimeter wavelengths when  $a_{\max} \sim 1$  mm.

Markov chain Monte Carlo (MCMC) fittings to the  $T_{\text{br}}$  profiles of TW Hya (Figure 1) were carried out to examine what  $a_{\max}$  values are indicated by such optically thick

( $\tau \gg 1$ ), isothermal and face-on thin dust slab model. In this case, MCMC is easier to implement than other fitting methods since every iteration of fittings needs to re-evaluate dust opacities based on the advanced  $a_{\max}$  value. The MCMC fittings were initialized with 100 walkers at the mean initial positions of [ $T_{\text{dust}} = 20$  K,  $a_{\max} = 0.1$  mm]. The walkers were iterated with 500 steps assuming flat priors; in the end, the results from the first 100 steps were discarded. These fittings achieved good convergence in the offset range of [-10, 10] AU except at the central location (i.e., offset=0 AU). Figure 4 shows the corner plot produced from the MCMC fittings at the 4.1 AU offset as an example of the convergence. The derived profiles of  $T_{\text{dust}}$  and  $a_{\max}$  from the MCMC fittings are presented in the top and bottom panels of Figure 1; the inferred  $\alpha$  values from the MCMC fittings are presented in the middle panel of Figure 1 but only for the offset range where the fittings converged well. Following Tsukagoshi et al. (2016), the top panel of Figure 1 also presents the  $T_{\text{dust}}(R) = 22$  [K]  $\times (R/10$  [AU]) $^{-0.4}$  and 28 [K]  $\times (R/10$  [AU]) $^{-0.4}$  midplane dust temperature profile models suggested from Andrews et al. (2012, 2016), where  $R$  denotes the radius. Note that the evaluation of these  $T_{\text{dust}}(R)$  models did not consider dust scattering with the potentially radially varying  $a_{\max}$ .

Results from the MCMC fittings show radially decreasing  $T_{\text{dust}}$ , which is everywhere higher than the observed  $T_{\text{br}}$  at Bands 4 and 6 but yet appear reasonable. Values of the derived  $a_{\max}$  radially decrease from  $\sim 100$   $\mu\text{m}$  to  $\sim 20$   $\mu\text{m}$ .

The dominant errors of the derived  $T_{\text{dust}}$  and  $a_{\max}$  are systematic, which were induced by the uncertainties of  $\kappa_{\nu}^{\text{abs}}$  and  $\kappa_{\nu}^{\text{sca,eff}}$ . They depend on the dust composition and the exact form of grain size distribution (e.g. Sierra et al. 2017; Soon et al. 2017), which are beyond the scope of the present work and is not quantitatively assessed. In addition, the MCMC fittings have poor convergence outside of the offset range of [-10, 10] AU and at the central location. These poor convergences can be understood, since outside of the offset range of [-10, 10] AU, the observed  $\alpha$  is becoming higher than 2.0, and that the optically thick assumption may not be valid at Band 4 (also see Figure 3 of Tsukagoshi et al. 2016). In addition, TW Hya presents a low density cavity around the central location (Figure 6; see also Andrews et al. 2016). The measured  $T_{\text{br}}$  at the central location at 0''.085 resolution was, therefore, subject to significant beam dilution. This led to degenerated fitting results of MCMC, which nevertheless reflect that the actual  $T_{\text{dust}}$  should be higher than the beam diluted  $T_{\text{br}}$  measurements.

Why the application of the geometrically thin dust slab solution of Birnstiel et al. (2018) can be self-consistently a good approximation? Does scattering of the warm dust emission from the central part of the disk in turn steepen the spectral index? We argue that the geometrically thin dust slab solution is indeed a good approximation for the case of TW Hya

due to that the derived temperature variations in the region of our interests (e.g.,  $\sim$ 0-10 AU radii) is not large. This is partly thanks to that TW Hya does not have a hot inner disk which is luminous at (sub)millimeter bands. Instead, the (sub)millimeter images of TW Hya presents an inner cavity. When the observed temperature variations and temperature gradients are not huge, and when the disk is geometrically thin, it is possible break down the global radiative transfer solution to a quasi-local problem. In the case that the temperature gradient is small, we can consider the temperature of the thin slab to be *locally uniform*. The adjacent disk components which are emitting at very different temperatures would have rather large spatial separations from the local component of interest, will see the local component at an asymptotically small solid angle, hence cannot contribute to significant scattered light flux.

To verify these arguments, we have carried out simple three dimensional radiative transfer simulations using the RADMC-3D code<sup>2</sup>, and compared the results from simulations with and without switching on dust scattering. In our RADMC-3D models, the radial gas column density ( $\Sigma_g$ ) profile was assumed to be

$$\Sigma_g [\text{g cm}^{-2}] = 4 \cdot 10^3 \times \left( \frac{r}{[\text{AU}]} \right)^{-0.5}, \quad (1)$$

where  $r$  is the projected radius on the disk midplane. The gas volume density ( $\rho$ ) were estimated based on

$$\rho [\text{g cm}^{-3}] = \Sigma_g \cdot \frac{1}{\sqrt{2\pi}h} e^{-\frac{z^2}{2h}}, \quad (2)$$

where  $z$  is the vertical offset from the disk midplane, and  $h$  is the characteristic disk scale height which we assumed as

$$h [\text{AU}] = 0.05 \cdot \left( \frac{r}{[\text{AU}]} \right)^{1.1}. \quad (3)$$

We truncated the column density profile inner than the 1 AU radius to mimic the presence of a inner cavity in TW Hya; our simulation covered a up to 20 AU radius. We assumed a constant 0.01 dust-to-gas mass ratio, and assumed a constant  $a_{\max} = 0.1$  mm. Our dust density model is therefore a geometrically thin disk with modestly small flaring, which is very optically thick in the inner 1~10 AU region and becomes optically thinner at outer radii. Testifying the geometrically thin assumption requires serious simulations of dust grain growth and dust vertical settling, which is by itself a developing research field and is well beyond the scope of the present paper. We assumed the dust temperature to be

$$T_{\text{dust}}(r, \phi, z) = 50 [\text{K}] \times \left( \frac{r}{[10 \text{ AU}]} \right)^{-0.4}, \quad (4)$$

where  $\phi$  is the azimuthal angle. Our simulations assumed similar temperature gradients with what was actually observed from TW Hya but a higher absolute temperature scale. This was because that our main purpose is to test whether or not including dust scattering can indeed lead to the anomalously low  $\alpha$  values. Using higher dust temperatures can avoid producing low  $\alpha$  values due to non-Rayleigh-Jeans effects. In addition, instead of evaluating dust temperature based on radiative transfer, we used the assumed radial temperature profile. Physically, this was because that on the spatial scales of our interests, how dust can be heated due to viscous dissipation is not yet certain. In addition, to simulate anisotropic dust scattering in the optically very thick limit, we need to use full three-dimension grids with rather small grid sizes, which makes the precise temperature evaluation computationally expensive and unfeasible for us. On the other hand, we do not want the simulations with and without dust scattering to converge to different temperature profiles, which will in turn confuse the discussion about the effects of dust scattering on  $\alpha$ .

The spatial grids of our simulations were defined in spherical coordinates with uniform intervals of polar angle, azimuthal angle, and logged radius. Using the RADMC-3D code, we derived the pole-on view of the disk at 232.990 GHz and 144.988 GHz. The simulated images have some numerical errors inward of the  $\sim$ 3 AU radius due to the very rapid changes of dust volume density with the radius and polar angle, which can lead to  $\sim \pm 0.02$  errors of the derived spectral indices. Therefore, we masked the inner 3.2 AU radius in the simulated images. Figure 5 shows the derived  $\alpha$  distributions from these simulations in the cases with and without switching on scattering. Indeed, in the case without switching on scattering,  $\alpha$  converges to 2.0 in the innermost, high optical depth region; when scattering was switched on,  $\alpha$  can converge to values lower than 2.0, which supports our arguments to apply the analytic thin slab solution.

### 3. DISCUSSION

Tsukagoshi et al. (2016) reported that  $\alpha$  has a value  $\sim$ 3.7 at the  $\sim$ 22 AU gap where the dust emission is relatively optically thin. This result is consistent with  $a_{\max} < 0.1$  mm (see Figure 4 of Birnstiel et al. 2018), and can be reconciled with the  $a_{\max}$  derived by present work at smaller radii without requiring a rapid spatial variation of  $a_{\max}$ . Tsukagoshi et al. (2016) suggested a shortage of millimeter size grains in the 22 AU gap. With the present work, it is also not clear where the millimeter size grains are presented inner than the 22 AU gap. Physically, even in the case that grown dust can efficiently form in regions inner than the 22 AU gap, whether or not we can detect the grown dust from observations remain questionable. For example, the simulations of Vorobyov et al. (2018) have shown that under certain phys-

<sup>2</sup> <http://www.ita.uni-heidelberg.de/~dullemond/software/radmc-3d/>

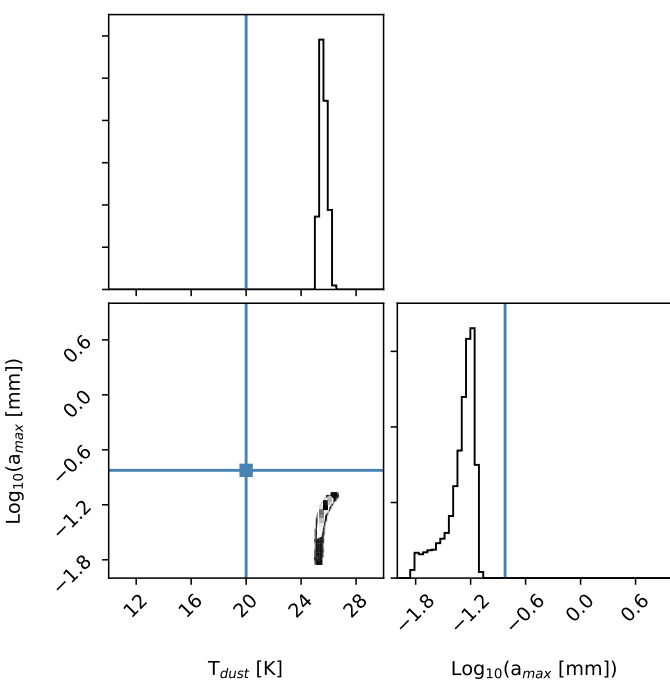


**Figure 4.** Corner plot for the results of MCMC fittings at 4.1 AU offset. Blue lines show the mean initial position of the MCMC walkers.

ical conditions, grown dust can have rapid radial migration and can be trapped to regions which have too small areas to be sensed by observations. The observations may also preferentially detect small dust grains at the scattering surface, due to the vertical settling of large dust grains (e.g., Yang et al. 2017; Hull et al. 2018; Dent et al. 2019).

The  $a_{\max}$  values derived in the present work (Figure 1) have no tension with those derived from the previous (sub)millimeter polarimetric observations (50–150  $\mu\text{m}$ ; Kataoka et al. 2016a,b; Hull et al. 2018). In this sense, the presented  $\alpha$  values and dust polarization in HD 163296 (Dent et al. 2019) may concordantly indicate to 10–100  $\mu\text{m}$  maximum grain sizes. In fact, resolving  $\alpha$  at multiple wavelengths may serve as a cheap (in terms of observing time) auxiliary method to help assess whether or not the observed dust linear polarization at a specific wavelength is dominated by dust scattering.

On the other hand, assuming that  $a_{\max}$  is still smaller in Class 0/I YSOs than in Class II protoplanetary disks, the previously observed dust linear polarization from Class 0/I YSOs may be preferably explained by aligned dust grains, which was supported by the highly consistent polarization percentages and position angles over broad ranges of wavelengths (e.g., Liu et al. 2016; Alves et al. 2018; Liu et al. 2018a; Sadavoy et al. 2018). The hypothesis of small  $a_{\max}$

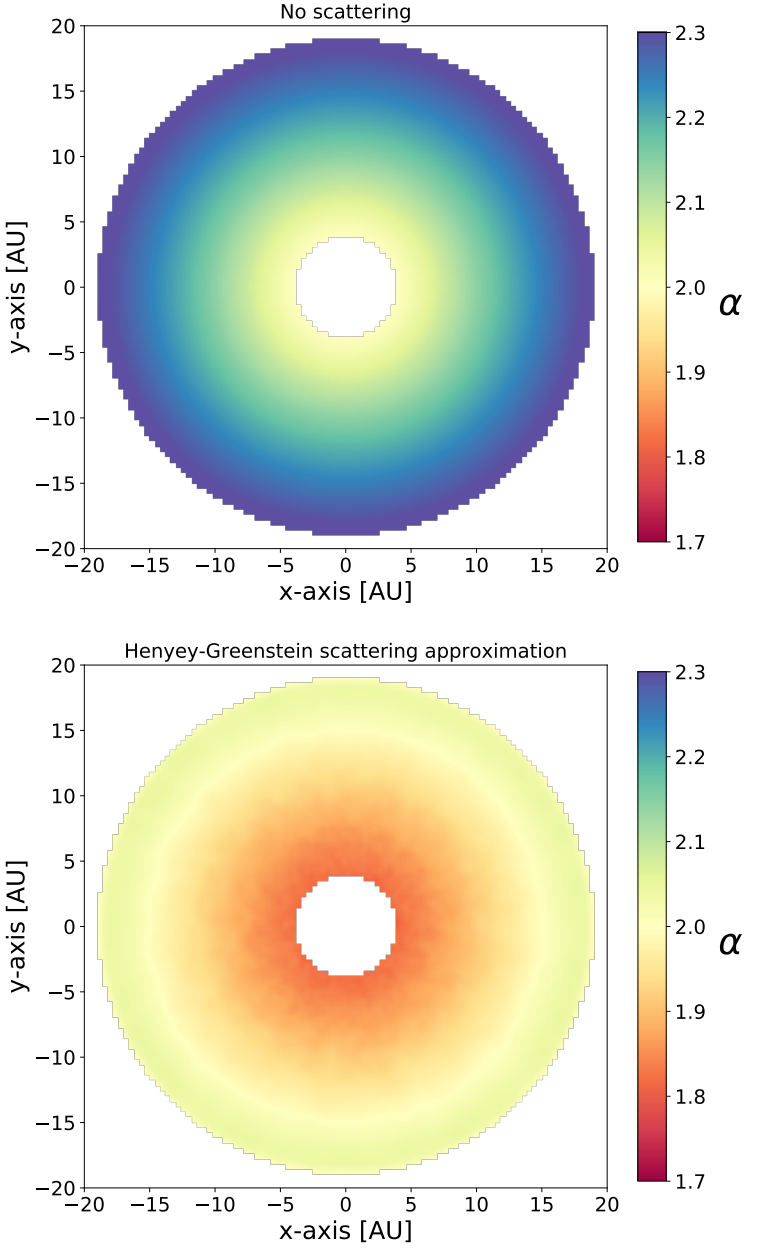


**Figure 5.** The spectral index ( $\alpha$ ) in between 144.988 GHz and 232.990 GHz derived from the RADMC-3D simulations for a face-on disk. Top and bottom panels show the cases with no scattering and with anisotropic scattering evaluated based on Heney-Greenstein approximation, respectively. These simulations were based on the identical assumption of density and temperature distributions (see Section 2).

values was also independently supported by astrochemical studies (Harada et al. 2017).

Finally, we recast that when albedo is high, the observed dust brightness temperature can be considerably lower than the actual (or expected) dust temperature even when the dust optical depth is much higher than 1 (Birnstiel et al. 2018).

When fitting the millimeter SED with a program that does not take scattering opacity into account, the fittings may be driven to conclude optically thin dust with significant grain growth, which can, in turn, lead to an underestimate of the total mass of solids.

HBL thanks the referee for the comments out of very critical thinking. This paper makes use of the following ALMA data: ADS/JAO.ALMA #2013.1.00114.S, #2015.1.00005.S. ALMA is a partnership of ESO (representing its member states), NSF (USA) and NINS (Japan), together with NRC (Canada), MOST and ASIAA (Taiwan), and KASI (Republic of Korea), in cooperation with the Republic of Chile. The Joint ALMA Observatory is operated by ESO, AUI/NRAO and NAOJ. This work has made use of data from the Eu-

ropean Space Agency (ESA) mission *Gaia* (<https://www.cosmos.esa.int/gaia>), processed by the *Gaia* Data Processing and Analysis Consortium (DPAC, <https://www.cosmos.esa.int/web/gaia/dpac/consortium>). Funding for the DPAC has been provided by national institutions, in particular the institutions participating in the *Gaia* Multilateral Agreement. HBL thanks Yasuhiro Hasegawa, Ryo Tazaki, and Mario Flock for the very useful discussion. H.B.L. is supported by the Ministry of Science and Technology (MoST) of Taiwan (Grant Nos. 108-2112-M-001-002-MY3 and 108-2923-M-001-006-MY3).

*Facility:* ALMA

*Software:* CASA (McMullin et al. 2007), Numpy (Van Der Walt et al. 2011), emcee (Foreman-Mackey et al. 2013), RADMC-3D (Dullemond et al. in prep.)

## REFERENCES

Aguirre-Gangas, C., Pineda, J. E., Szucs, L., et al. 2019, arXiv e-prints, [arXiv:1901.05021 \[astro-ph.SR\]](https://arxiv.org/abs/1901.05021)

Alves, F. O., Girart, J. M., Padovani, M., et al. 2018, *A&A*, 616, A56

Andrews, S. M., Wilner, D. J., Hughes, A. M., et al. 2012, *ApJ*, 744, 162

Andrews, S. M., Wilner, D. J., Zhu, Z., et al. 2016, *ApJL*, 820, L40

Bacciotti, F., Girart, J. M., Padovani, M., et al. 2018, *ApJL*, 865, L12

Beckwith, S. V. W., & Sargent, A. I. 1991, *ApJ*, 381, 250

Birnstiel, T., Dullemond, C. P., Zhu, Z., et al. 2018, *ApJL*, 869, L45

Carrasco-González, C., Henning, T., Chandler, C. J., et al. 2016, *ApJL*, 821, L16

Dent, W. R. F., Pinte, C., Cortes, P. C., et al. 2019, *MNRAS*, 482, L29

Foreman-Mackey, D., Hogg, D. W., Lang, D., & Goodman, J. 2013, *PASP*, 125, 306

Gaia Collaboration, Brown, A. G. A., Vallenari, A., et al. 2016, *A&A*, 595, A2

—. 2018, *A&A*, 616, A1

Galván-Madrid, R., Liu, H. B., Izquierdo, A. F., et al. 2018, *ApJ*, 868, 39

Harada, N., Hasegawa, Y., Aikawa, Y., et al. 2017, *ApJ*, 837, 78

Hildebrand, R. H. 1983, *QJRAS*, 24, 267

Huang, J., Andrews, S. M., Cleeves, L. I., et al. 2018, *ApJ*, 852, 122

Hull, C. L. H., Yang, H., Li, Z.-Y., et al. 2018, *ApJ*, 860, 82

Jørgensen, J. K., Bourke, T. L., Myers, P. C., et al. 2007, *ApJ*, 659, 479

Kataoka, A., Muto, T., Momose, M., Tsukagoshi, T., & Dullemond, C. P. 2016a, *ApJ*, 820, 54

Kataoka, A., Muto, T., Momose, M., et al. 2015, *ApJ*, 809, 78

Kataoka, A., Tsukagoshi, T., Momose, M., et al. 2016b, *ApJL*, 831, L12

Li, J. I., Liu, H. B., Hasegawa, Y., & Hirano, N. 2017, *ApJ*, 840, 72

Liu, H. B., Hasegawa, Y., Ching, T.-C., et al. 2018a, *A&A*, 617, A3

Liu, H. B., Galván-Madrid, R., Forbrich, J., et al. 2014, *ApJ*, 780, 155

Liu, H. B., Lai, S.-P., Hasegawa, Y., et al. 2016, *ApJ*, 821, 41

Liu, H. B., Vorobyov, E. I., Dong, R., et al. 2017, *A&A*, 602, A19

Liu, H. B., Dunham, M. M., Pascucci, I., et al. 2018b, *A&A*, 612, A54

McMullin, J. P., Waters, B., Schiebel, D., Young, W., & Golap, K. 2007, *adass*, 376, 127

Miotello, A., Testi, L., Lodato, G., et al. 2014, *A&A*, 567, A32

Qi, C., Ho, P. T. P., Wilner, D. J., et al. 2004, *ApJL*, 616, L11

Roberge, A., Weinberger, A. J., & Malumuth, E. M. 2005, *ApJ*, 622, 1171

Sadavoy, S. I., Myers, P. C., Stephens, I. W., et al. 2018, *ApJ*, 869, 115

Sierra, A., Lizano, S., & Barge, P. 2017, *ApJ*, 850, 115

Soon, K.-L., Hanawa, T., Muto, T., Tsukagoshi, T., & Momose, M. 2017, *PASJ*, 69, 34

Stephens, I. W., Yang, H., Li, Z.-Y., et al. 2017, *ApJ*, 851, 55

Tsukagoshi, T., Nomura, H., Muto, T., et al. 2016, *ApJL*, 829, L35

Van Der Walt, S., Colbert, S. C., & Varoquaux, G. 2011, ArXiv e-prints, [arXiv:1102.1523 \[cs.MS\]](https://arxiv.org/abs/1102.1523)

Vorobyov, E. I., Akimkin, V., Stoyanovskaya, O., Pavlyuchenkov, Y., & Liu, H. B. 2018, *A&A*, 614, A98

Yang, H., Li, Z.-Y., Looney, L. W., Girart, J. M., & Stephens, I. W. 2017, *MNRAS*, 472, 373

## APPENDIX

## A. REPRODUCING ALMA MEASUREMENTS

The archival ALMA Band 4 and 6 data were re-calibrated and phase self-calibrated following the strategy outlined in Section 2 of [Tsukagoshi et al. \(2016\)](#), using the CASA software package v5.4.0 ([McMullin et al. 2007](#)). The continuum data were derived using the CASA-`uvcontsub` task. The Band 4 and Band 6 continuum data were imaged separately, using the multi-frequency synthesis (MFS) method. Different from [Tsukagoshi et al. \(2016\)](#), this work employed  $n_{term}=1$  in MFS and did not employ multiscale clean, to avoid the systematic flux errors induced by spectral index errors and by non-local imaging artifacts. The Band 6 image achieved a  $\theta_{\text{maj}} \times \theta_{\text{min}} = 0''.075 \times 0''.064$  synthesized beam and a  $23 \mu\text{Jy beam}^{-1}$  root-mean-square (RMS) noise level; the Band 4 image achieved a  $\theta_{\text{maj}} \times \theta_{\text{min}} = 0''.081 \times 0''.058$  synthesized beam and a  $14 \mu\text{Jy beam}^{-1}$  RMS noise level. The achieved images are presented in Figure 6. Afterward, these images were smoothed to have  $0''.085$  ( $\sim 5.1$  AU) circular beams before the following analysis.

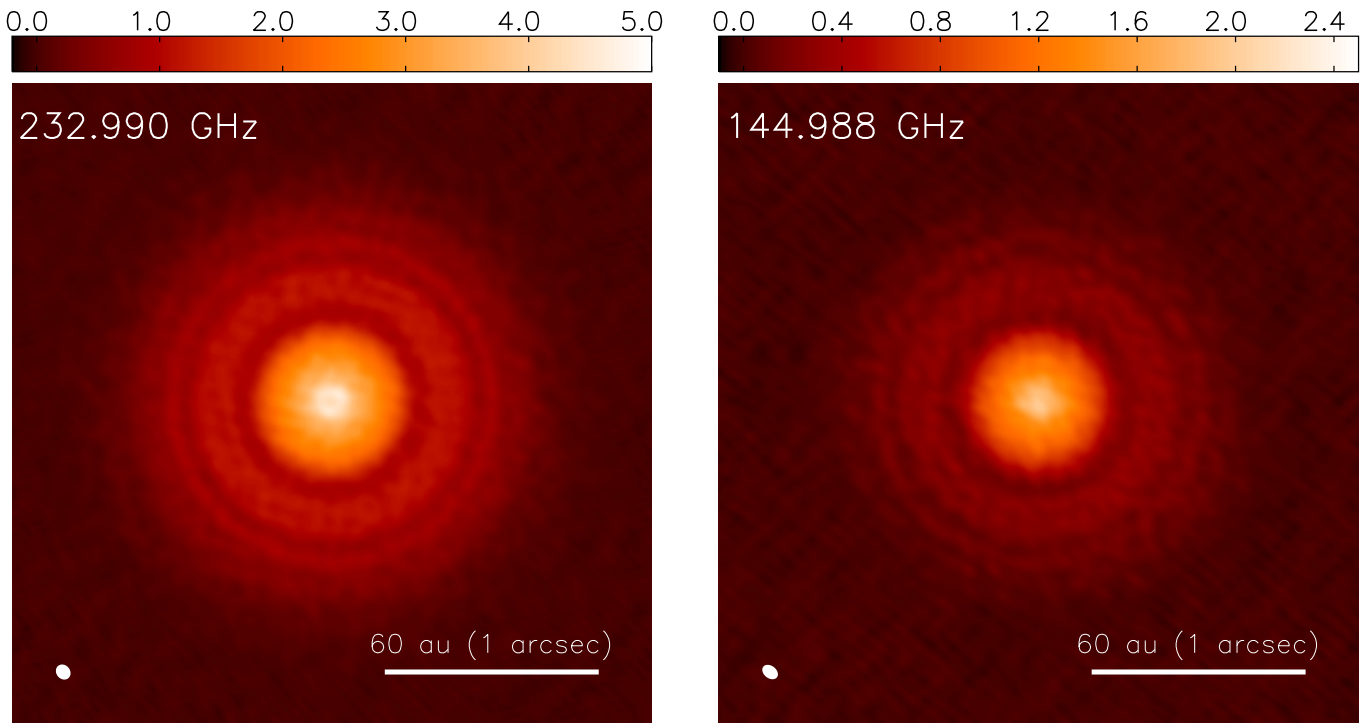


**Figure 6.** ALMA 232.990 GHz (Band 6) and 144.988 GHz (Band 4) images of TW Hya in units of  $\text{mJy beam}^{-1}$ . The synthesized beams at Band 6 and 4 are  $\theta_{\text{maj}} \times \theta_{\text{min}} = 0''.075 \times 0''.064$  (P.A.= $39^\circ$ ) and  $\theta_{\text{maj}} \times \theta_{\text{min}} = 0''.081 \times 0''.058$  (P.A.= $52^\circ$ ), respectively. They are shown in bottom left of individual panels. The RMS noise level of the Band 6 and 4 images are  $23 \mu\text{Jy beam}^{-1}$  and  $14 \mu\text{Jy beam}^{-1}$ , respectively.